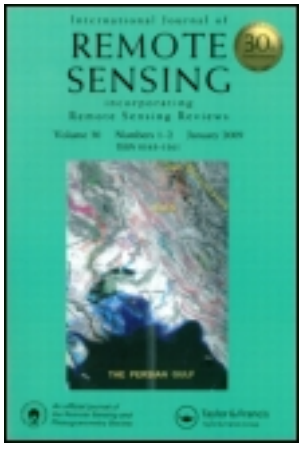


International Journal of Remote Sensing

Publication details, including instructions for authors and subscription information:
http://www.tandfonline.com/loi/tres20

# Integration of multitemporal/polarization C-band SAR data sets for land-cover classification

N.-W. Park [a] & K.-H. Chi [a]

[a] Geoscience Information Center, Korea Institute of Geoscience and Mineral Resources, 30 Gajeong-dong, Yuseong-gu, Daejeon 305-350, Korea

Version of record first published: 23 Jul 2008.

To cite this article: N.-W. Park & K.-H. Chi (2008): Integration of multitemporal/polarization C-band SAR data sets for land-cover classification, International Journal of Remote Sensing, 29:16, 4667-4688

To link to this article: http://dx.doi.org/10.1080/01431160801947341

*International Journal of Remote Sensing*
Vol. 29, No. 16, 20 August 2008, 4667–4688

Taylor & Francis
Taylor & Francis Group

# Integration of multitemporal/polarization C-band SAR data sets for land-cover classification

N.-W. PARK* and K.-H. CHI

Geoscience Information Center, Korea Institute of Geoscience and Mineral Resources, 30 Gajeong-dong, Yuseong-gu, Daejeon 305-350, Korea

(*Received 20 December 2006; in final form 1 August 2007*)



This paper investigates the potential of multitemporal/polarization C-band SAR data for land-cover classification. Multitemporal Radarsat-1 data with HH polarization and ENVISAT ASAR data with VV polarization acquired in the Yedang plain, Korea are used for the classification of typical five land-cover classes in an agricultural area. The presented methodologies consist of two analytical stages: one for feature extraction and the other for classification based on the combination of features. Both a traditional SAR signal property analysis-based approach and principal-component analysis (PCA) are applied in the feature extraction stage. Special concerns are in the interpretation of each principal component by using principal-component loading. The tau model applied as a decision-level fusion methodology can provide a formal framework in which the posteriori probabilities derived from different sensor data can be combined. From the case study results, the combination of PCA-based features showed improved classification accuracy for both Radarsat-1 and ENVISAT ASAR data, as compared with the traditional SAR signal property analysis-based approach. The integration of PCA-based features based on multiple polarization (i.e. HH from Radarsat-1, and both VV and VH from ENVISAT ASAR) and different incidence angles contributed to a significant improvement of discrimination capability for dry fields which could not be properly classified by using only Radarsat-1 or ENVISAT ASAR data, and thus showed the best classification accuracy. The results of this case study indicate that the use of multiple polarization SAR data with a proper feature extraction stage would improve classification accuracy in multitemporal SAR data classification, although further consideration should be given to the polarization and incidence angle dependency of complex land-cover classes through more experiments.

## 1. Introduction

Terrain classification has been regarded as one of the most important application issues of remote sensing, since the classification results such as land-cover/use, ecological units, and lithology maps have been widely used in many environmental applications. In remote-sensing data classification, it is very important to select both a proper classification methodology and images acquired for a date of interest, or for when the discrimination between land-cover classes is best. The availability of optical data, however, heavily depends on weather conditions, and it is difficult or even impossible to get cloud-free data in the rainy season. The non-availability of

*Corresponding author. Email: nwpark@kigam.re.kr

*International Journal of Remote Sensing*
ISSN 0143-1161 print/ISSN 1366-5901 online 
http://www.tandf.co.uk/journals
DOI: 10.1080/01431160801947341

cloud-free optical data is consequently an obstacle to timely analysis in areas of interest.

From the availability aspect, SAR data provide us with an unprecedented opportunity for Earth observation. Despite its advantages, however, it is very difficult to obtain satisfactory classification accuracy when compared with that of optical data. This lesser capability results from several causes, which include speckle noise, geometric distortion consequent upon a side-looking imaging system and single polarization of available spaceborne SAR data such as ERS, JERS-1, and Radarsat-1. The sole use of backscattering coefficients for single polarization SAR data could not achieve satisfactory classification accuracy, notwithstanding the incorporation of other information such as texture derived from SAR backscattering coefficients (Carr and Miranda 1998).

To overcome the difficulty in SAR data classification, some additional or complementary features in addition to backscattering coefficients can be considered. Multitemporal SAR data permit an account for the temporal variation of the SAR signal and also an extraction of additional information on land-cover class, under the assumption that there has been no transition between land-cover classes during the considered period but only a change in physical conditions (Askne and Hagberg 1993, Angelis *et al.* 2002). By analysing the temporal behaviour of various land-cover classes from multitemporal data, an improvement of the thematic information content of backscattering coefficients can be achieved (Wegmüller *et al.* 2003). For example, land-cover classes with many changes in their physical condition (e.g. water and cultivated areas) can be discriminated from those with a low temporal variability (e.g. forest and urban areas). Interferometric coherence that can also be extracted from multitemporal data is a valuable information source with potential for application in the determination of temporal stability of land-cover classes. Urban areas generally show a higher temporal stability than most natural targets, and so they can be discriminated from others. See Strozzi *et al.* (2000) for a detailed description on the typical characteristics of features from multitemporal interferometric SAR data analysis.

Previous studies (Strozzi *et al.* 2000, Engdahl and Hyyppä 2003, Bruzzone *et al.* 2004) have used ERS-1/2 SAR Tandem pairs and shown the potential of those data for land-cover classification. These data cannot now be further obtained, and time series of previously obtained ERS-1/2 Tandem pairs are very rare in the Asian area including Korea. JERS-1 SAR data acquired with a 44-day interval from 1992 to 1998 and the currently operating Radarsat-1 data with a 24-day interval are generally available in that region. These JERS-1 and Radarsat-1 data still provide us with single frequency and polarization information. The information deficit due to single frequency and/or polarization data may be relieved by not only the new generation of SAR sensors delivering the dual polarization data of ENVISAT ASAR, the fully polarimetric data of ALOS PALSAR and Radarsat-2, but also the combination of traditional SAR sensors. Some experiments with fully polarimetric airborne SAR data showed that the fully polarimetric SAR data could give more detailed information on land-cover classes and thus improve the discrimination capability of land-cover classes (Cloude and Pottier 1997, Freeman and Durden 1998, Ferro-Famil *et al.* 2001, Lee *et al.* 2001). Despite its great potential, the integrated analysis of multiple frequency and/or polarization spaceborne SAR data has not as yet been in conjunction with land-cover classification with multitemporal spaceborne SAR data.

To fully use the complementary information on the land-cover classes which can be derived from the multitemporal/polarization SAR data sets, an effective classification methodology for dealing with this information should also be developed. Among various data-integration methodologies, a tau model which has been proposed by Journel (2002) can effectively integrate several posteriori probabilities derived from multiple sources or sensors. Unlike the traditional Bayesian combination approach, the distance from the a priori probability for each of the data is first defined, and then the final joint posteriori probability is derived in this model. This model conceptually takes into account data redundancy between the data utilized. Despite its simplicity and applicability to multiple data integration, so far it has only been applied to geological applications (Caers *et al.* 2001, Krishnan 2004) and it has not as yet been tested for land-cover classification with multisensor data.

The potential of multitemporal/polarization C-band SAR data for land-cover classification is investigated in this paper. Multitemporal Radarsat-1 data with HH polarization and ENVISAT ASAR data with VV polarization are used in this study. The proposed framework is based on a two-stage approach that includes feature-extraction and combination stages (figure 1). On the feature-extraction stage, both the traditional feature-extraction approach based on SAR signal property analysis and principal-component analysis (PCA) are applied and compared. PCA is especially adopted to investigate a possibility of the extraction of specific information relevant to land-cover classification. The tau model is applied as a decision-level fusion methodology on the second feature combination stage for

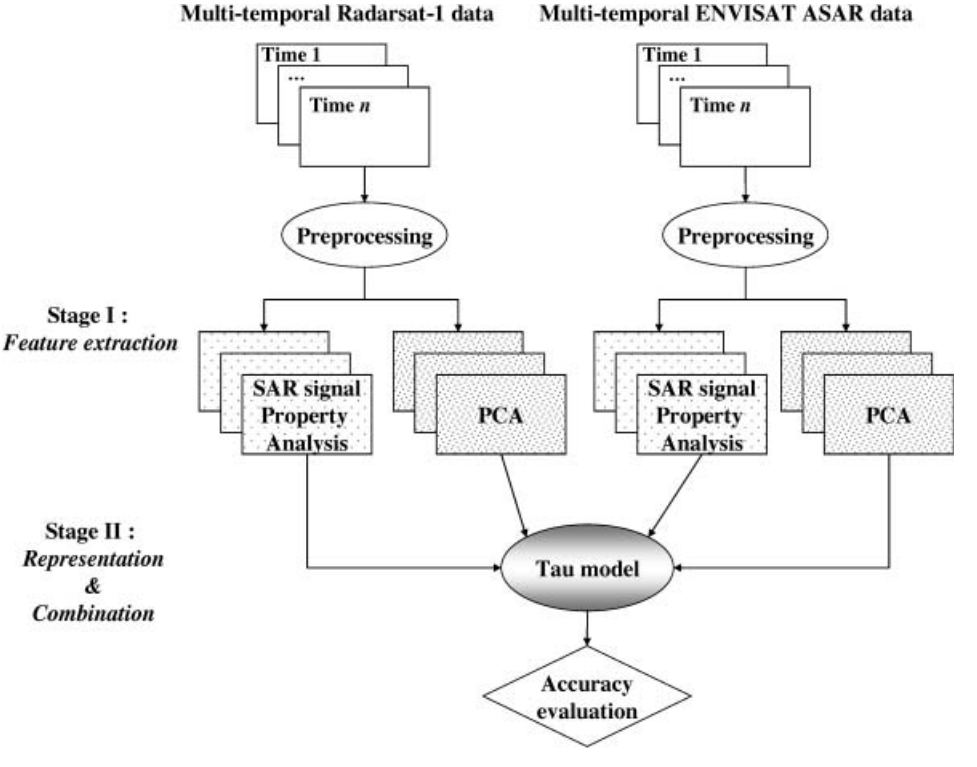


Figure 1. Schematic diagram of the processing flow applied in this study.

classification. A case study of supervised land-cover classification for a Korean agricultural area is described to illustrate the applicability of the proposed framework for land-cover classification.

## 2. Study area and data sets

The present study was conducted at the Yedang plain of Korea where multitemporal SAR data have been acquired (figure 2). The multitemporal data sets for Radarsat-1 and ENVISAT ASAR used in this study are listed in table 1. The nine Radarsat-1 data acquired from April 2005 to October 2005 were used with an ENVISAT ASAR data set, which spans a whole year from October 2004 to October 2005. The

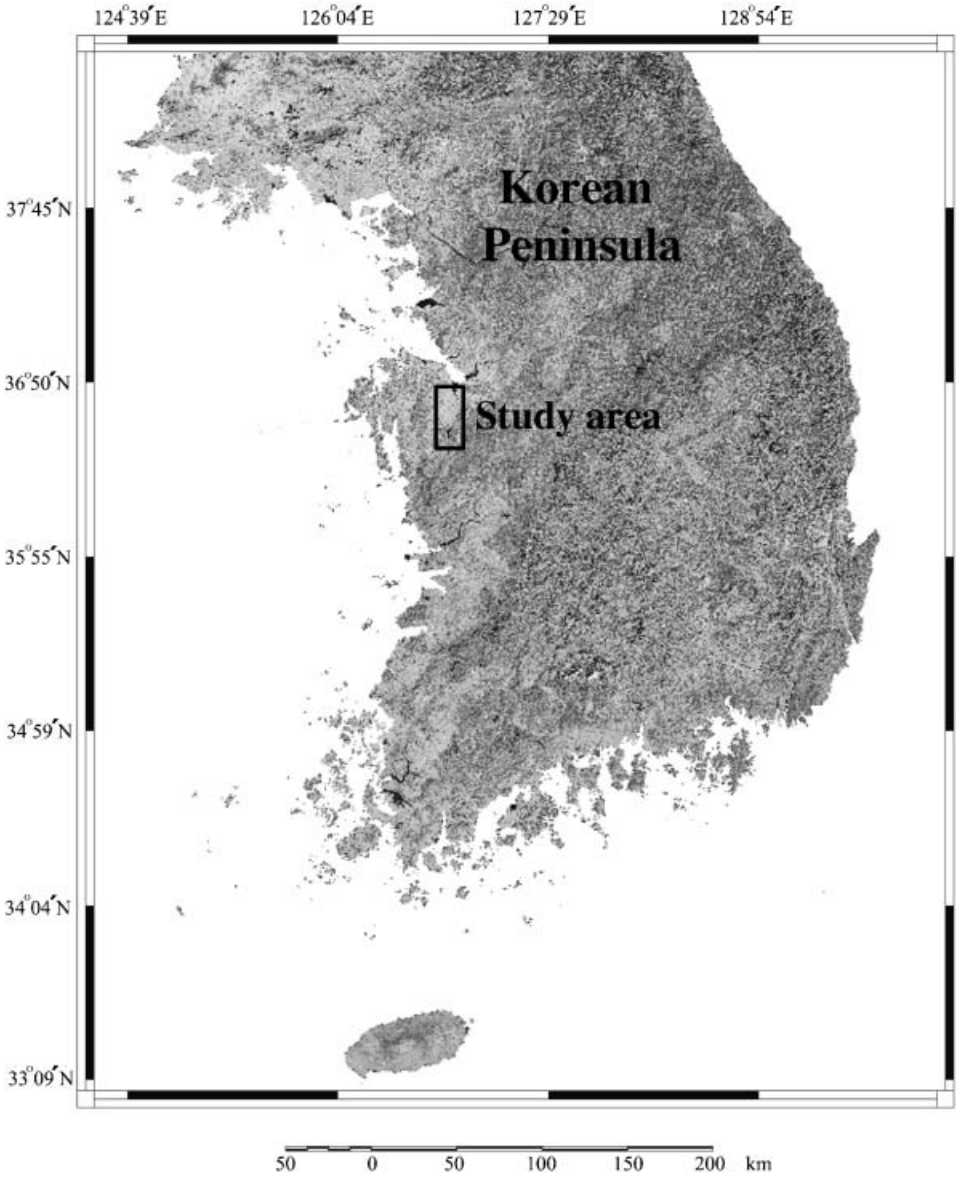


Figure 2. Location of the study area.

Table 1. List of multitemporal SAR data sets used in this study.

| Sensor | Date | Mode (incidence angle) | Polarization |
|---|---|---|---|
| Radarsat-1 | 1 April 2005 | Ascending F2 (40°) | HH |
| | 25 April 2005 | | |
| | 19 May 2005 | | |
| | 12 June 2005 | | |
| | 6 July 2005 | | |
| | 30 July 2005 | | |
| | 23 August 2005 | | |
| | 16 September 2005 | | |
| | 10 October 2005 | | |
| ENVISAT ASAR | 31 October 2004 | Descending IS2 (23°) | VV |
| | 9 January 2005 | | |
| | 13 February 2005 | | |
| | 20 March 2005 | | |
| | 24 April 2005 | | |
| | 29 May 2005 | | VV & HH |
| | 17 June 2005 | Descending IS1 (19°) | VV & VH |
| | 3 July 2005 | Descending IS2 (23°) | VV |
| | 7 August 2005 | | |
| | 11 September 2005 | | |
| | 16 October 2005 | | |



ENVISAT ASAR data set included two products acquired in the alternating polarization mode. These images acquired on 29 May 2005 and 17 June 2005 have co-polarization (VV and HH), and cross-polarization (VV and VH), respectively. As shown in table 1, the Radarsat-1 and ENVISAT ASAR data sets have differing incidence angles and polarization. The scattering response depends on both of these factors, and various land-cover classes would reflect the different importance of this dependence (Ulaby and Dobson 1988). The higher incidence angle of Radarsat-1 (i.e. 40°) than the 23° of ENVISAT ASAR has the possibility of improving the thematic information content by reducing geometric distortion and improving the discrimination of open water (Wegmüller *et al.* 2003). As a result, the integration of multitemporal data sets including Radarsat-1 and ENVISAT ASAR in this case study corresponds to the integration of multitemporal data sets with different incidence angles and polarization states.

All data used were in the single-look complex (SLC) format, and several preprocessing techniques for these data were carried out by using the SARScape software (SARMAP, Switzerland). Multilooking was undertaken to generate intensity images by averaging the power across a number of lines in both the azimuth and range directions. Five azimuth looks were applied to ENVISAT ASAR data by considering the data-acquisition geometry. For the Radarsat-1 data, three looks in range and four in azimuth were applied to generate the same spatial resolution data as ENVISAT ASAR data (i.e. approximately square pixels of 25-m resolution). Coregistration with sub-pixel accuracy was undertaken automatically by using orbit information and a cross-correlation algorithm. Speckle noise was reduced by applying time-series filtering, which can preserve the spatial resolution and significantly increase the signal-to-noise ratio (De Grandi *et al.* 1997). Since the Radarsat-1 and ENVISAT ASAR data were acquired from different viewing directions (i.e. ascending and descending orbits), they showed a different imaging geometry. To reduce the effect of topography on the backscattering coefficient, a

geocoding with DEM extracted from a 1 : 25 000 scale digital topographic map of the study area was done. The layover and shadow zones that were extracted during geocoding were masked out throughout the classification data processing.

The five land-cover classes including paddy fields, dry fields, forest, water, and built-up areas were considered in this study. In previous studies (Strozzi *et al.* 2000, Bruzzone *et al.* 2004), the cultivated areas have included both paddy and dry fields. Although paddy and dry fields are likely to show a higher temporal variability than that of other classes, the intensity or properties of temporal variability between those two cultivated areas may be quite different due to different cultivation mechanisms applied during the plant growth cycle. In this study, the paddy and dry fields were considered as separate land-cover types.

For the supervised classification, reference data were collected during field surveys from July 2005 to October 2005. High-resolution optical data acquired in April and June 2005 were also used for construction of the reference data. The reference data were randomly partitioned into training (11 037 pixels) and validation sets (9546 pixels). The original validation set included a large number of paddy fields and water classes (5200 and 1923 pixels, respectively). This large portion of these two classes may lead to biased classification accuracy and affect accuracy statistics of other classes. Thus, small portions of the two classes (1255 and 328 pixels, respectively) were selected by considering the portions of other classes. The final validation set of 4000 pixels was used for accuracy assessment.



## 3. Methodology

### 3.1 *Feature extraction*

In multitemporal SAR data analysis for land-cover classification, a feature extraction stage is first considered, and thereafter classification and assessment are carried out. Two feature-extraction approaches including both traditional SAR signal property analysis and PCA are separately applied.

The first feature-extraction approach is based on SAR signal property analysis. This approach extracts features by considering the temporal variation of backscattering coefficients and information from interferometric data processing (Strozzi *et al.* 2000). Park *et al.* (2005) tested the variation of classification accuracy with respect to various combination cases of the average backscattering coefficient, temporal variability, and long-term coherence extracted from multitemporal Radarsat-1 data in an agricultural area. The best classification accuracy was obtained from a combination of all three features. Based on our previous results, this study considers the above three features, and brief descriptions of these are given hereafter.

The average backscattering coefficient permits the distinction of water and urban classes due to their respective very low and high signatures. However, the value of forest and cultivated areas tends to overlap significantly, and so the discrimination of those classes may not be clear. Temporal variability, which is a main feature in multitemporal analysis, can be used to distinguish cultivated areas and water from the forest and urban classes. It should be noted that the relative magnitude of temporal variability depends on factors such as frequency, polarization, and incidence angle of the SAR sensor considered. For example, the temporal variability of water is generally higher in VV than that in the HH polarization data. The standard deviation values were considered as a measure of temporal variability in this study.

As a final feature, long-term coherence is used to obtain information on the discrimination of urban areas where there are many permanent scatterers from other classes. The texture of backscattering intensity may be considered in the discrimination of urban areas. As discussed in Bruzzone *et al.* (2004), a degradation of spatial resolution occurs due to the ensemble averaging procedure for texture derivation. Conversely, information with better urban area resolution can be achieved from the long-term coherence. For this reason, long-term coherence is considered in this study. The long-term C-band coherence was computed and averaged from image pairs with a temporal baseline of 24 and 35 or more days, and with a short spatial baseline.

In addition to the indicated traditional features, if ENVISAT ASAR data are acquired in an alternating polarization mode, the polarization ratio can provide further thematic information. The ratio of VH and VV channels (VH/VV) acquired on 17 June 2005 was considered as another feature in this study.

It is worth noting that the features mentioned above provide complementary information on various land-cover classes. For example, the range of temporal variability in forest and urban areas may overlap, but the discrimination of the two classes may be improved by using long-term coherence or average backscattering coefficients because of their high values over urban areas. The above three features will be used together as the input for classification, since the main focus of this study is on the effect of using multiple polarization data on classification accuracy, not on determining the best feature combination case among features based on SAR signal property analysis

The second approach is to use features based on PCA. PCA is a statistical technique to transform a large number of data to optimal linear combinations (Tso and Mather 2001). Since the multitemporal data sets considered in this study include more than nine images and are somewhat correlated to one another, some principal components (PCs) among all of those transformed are used as input features for classification. Each PC in new feature space would contain particular information relevant to various land-cover classes. Thus, the focus of applying PCA is to determine which PC is useful for the discrimination of a particular land-cover class. Traditional PCA studies have selected a small number of data that are illustrated by a consideration of the eigenvalues that can account for an amount of total variance. However, the information content in each PC was not investigated fully for interpretation purposes. Although PCA is not a new algorithm for feature extraction or reduction, this study will demonstrate that PC loadings, which have not been used in traditional PCA-based image analysis, would be useful to interpret the contribution of each image to the PC, and thus PCA can be effectively applied to multiple SAR data analysis. The principal-component loadings, which are coefficients of the linear equation that the eigenvector defines, can provide a summary of the influence of the original data on the PC. The principal-component loadings were used in this study as a basis for the interpretation of each PC.

### 3.2 *Tau model*

The tau model, which provides a convenient way of combining the posteriori probabilities derived from different sources (Journel 2002), was applied as a decision-level fusion methodology. Instead of using the posteriori probabilities directly, the logistic-type ratio of the a priori and posteriori probabilities are considered in the tau model. Before integration by the tau model, the multilayer

perceptron neural network (MLP) with the error backpropagation learning algorithm was applied to derive the posteriori probabilities. According to a previous study (Richard and Lippmann 1991), a neural network trained by using a mean-square-error criterion provides estimates of posteriori probabilities. In this study, the posteriori probabilities for each sensor data are regarded as preposteriori probabilities for the tau model.

Suppose that we have already had an a priori probability $P(\omega_k)$ and the sensor-specific preposteriori probabilities ($P(\omega_k|D_{i.})$) derived from the $i$th SAR sensor for the target class $\omega_k$. $D_{i.}$ denotes a whole set of features extracted from the $i$th sensor. In our data set, $i$ takes two cases: one for Radarsat-1 and the other for ENVISAT ASAR. In the tau model, distances to the probability ratios (i.e. $a$ and $d_i$, respectively) of $P(\omega_k)$ and $P(\omega_k|D_{i.})$ are first defined by Journel (2002) and Krishnan (2004):

$$a = \frac{1 - P(\omega_k)}{P(\omega_k)}, \tag{1}$$

$$d_i = \frac{1 - P(\omega_k|D_{i.})}{P(\omega_k|D_{i.})}. \tag{2}$$

The ratio of the joint posteriori probability ($X$) and the final joint posteriori probability $P(\omega_k|D_{1.}, D_{2.})$ are then derived as:

$$X = a\prod_{i=1}^{2}\left(\frac{d_i}{a}\right)^{\tau_i},\ \tau_i \in [-\infty, +\infty], \tag{3}$$

$$P(\omega_k|D_{1.}, D_{2.}) = \frac{1}{1+X} \in [0, 1], \tag{4}$$

where $\tau_i$ is related to the redundancy between the information arriving from different sensor data. The ratio $\frac{d_i}{a}$ can be regarded as the incremental contribution of sensor $D_{i.}$ to that distance starting from the prior distance $a$. $X$ would be the distance to $\omega_k$ occurring after jointly observing data sets (Journel 2002).

In equation (3), weights $\tau_i$ only measure the additional contribution brought by any single data over that of all previously considered data (Krishnan 2004). As discussed in Krishnan (2004), they are dependent on both data sequence and data values, and so it is very complex to derive exact analytical expressions. If they are all set to unity, the above equation is equivalent to combination under conditional independence. They were assumed to be unity in this study, corresponding to the assumption of conditional independence between the Radarsat-1 and ENVISAT ASAR data sets. As for the assignment of land-cover class at each pixel, the maximum a posteriori decision rule was adopted.

## 4. Results and discussion

### 4.1 *Feature extraction results*

The different polarization SAR data sets were processed separately during the feature extraction stage, since some features could be extracted only from a particular data set. The nine Radarsat-1 data were used simultaneously both for the extraction of the average backscattering coefficient and temporal variability, and for PCA. The long-term coherence maps of Radarsat-1 data were also derived from two

interferometric pairs with a 24-day interval and three pairs with a 48-day interval, and then averaged. Three features extracted from the multitemporal Radarsat-1 data set are shown in figure 3. As expected, these features show the typical characteristics discussed in §3.

The eigenvalue plot of principal components and their loadings for the whole Radarsat-1 data are given in figure 4. From figure 4(*a*), we can know how much of the total variability is explained by the individual PC. The first three PCs together explain about 91% of the variance. Based on a visual check and the amount of total variance, the first three PCs were selected as features of PCA. The PC loading plot provides a convenient summary of the influence of the original data on the PC and is thus a useful basis for interpretation, as shown in figure 4(*b*). A large absolute value corresponds to a high loading, and that variable dominance affects the PC considered. The loadings for the first PC are all of the same sign and of moderate size. A reasonable interpretation is that this component represents an average score for the nine Radarsat-1 data. In the second PC, the May and June data have large absolute loading values. This means that the effect of May and June data results in the high value of the second PC image and can be discriminated from the values of remaining data. This implies that the second PC is similar to temporal variability. The third PC shows a gradual increase in values. The first three PCs are shown in figure 5. As described above, the first and second PCs are respectively similar to the average backscattering coefficient and temporal variability in figure 3. Although it is difficult to visually distinguish patterns from the third PC, it holds unique information that will be revealed through a histogram analysis between the pixel values in the third PC and training set.

Since the ENVISAT ASAR data set includes different polarization and/or mode data, some of these were included or excluded. The average backscattering coefficient and temporal variability were computed from 10 data items acquired from descending orbits with IS2 mode. Only the VV polarization channel within the

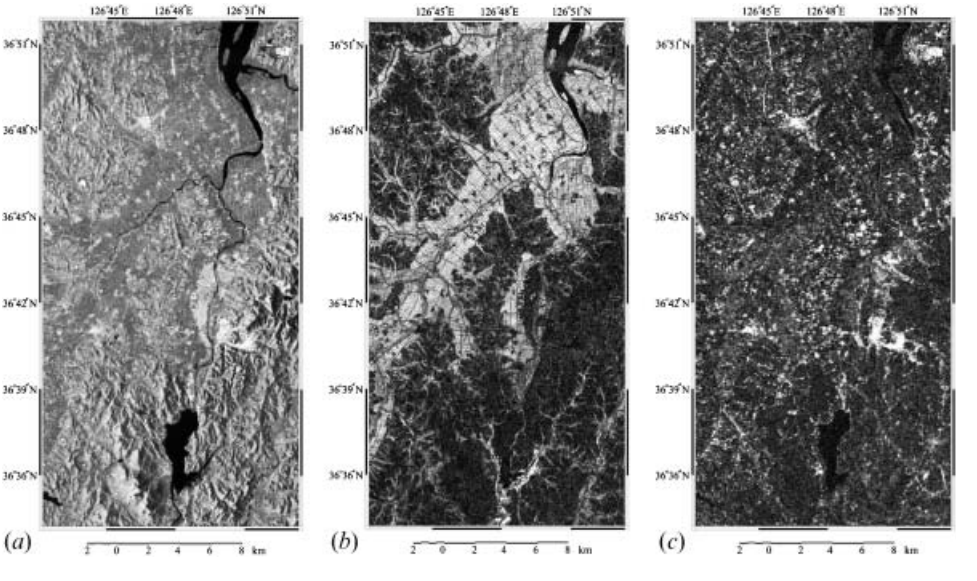


Figure 3. SAR signal property analysis-based features for Radarsat-1 data: (*a*) average backscattering coefficient, (*b*) temporal variability, (*c*) long-term oherence.

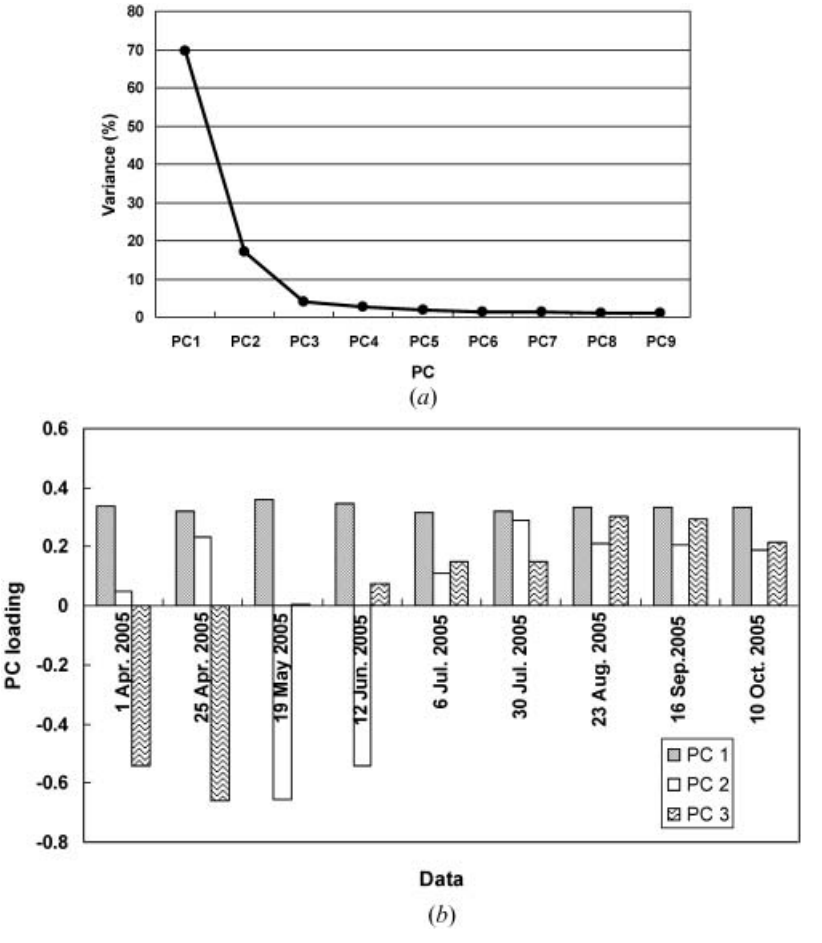


Figure 4. (*a*) Percentage of total variance explained by each PC of Radarsat-1 data and (*b*) principal-component loadings of input Radarsat-1 data.

dual polarization data acquired on 29 May 2005 was used for those features (figure 6). Unlike the temporal variability of the Radarsat-1 data set, a high temporal variability can be observed in both water and paddy fields. The differing intensity of temporal variability observed in the ENVISAT ASAR data is mainly due to a combination of VV polarization and a small incidence angle. However, all the ENVISAT ASAR data were used for PCA. The long-term coherence images were extracted from two interferometric pairs with a 35-day interval and then averaged.

From the eigenvalue analysis in PCA, the first three components that accounted for about 89% of the total variation were selected as PCA-based features, as in the case of the Radarsat-1 data set (figure 7(*a*)). An analysis of the PC loadings was also carried out to investigate the effect of each ENVISAT image on each PC (figure 7(*b*)). As with the Radarsat-1 results, the first PC has similar loading values for all data sets. This means that the first PC is similar to the mean of the time series. In the second PC, data acquired in May and June showed large negative loading values from the dominant effect of wet paddy fields. A large value for data acquired in October 2005 was also observed. Harvesting was carried out at that time in the

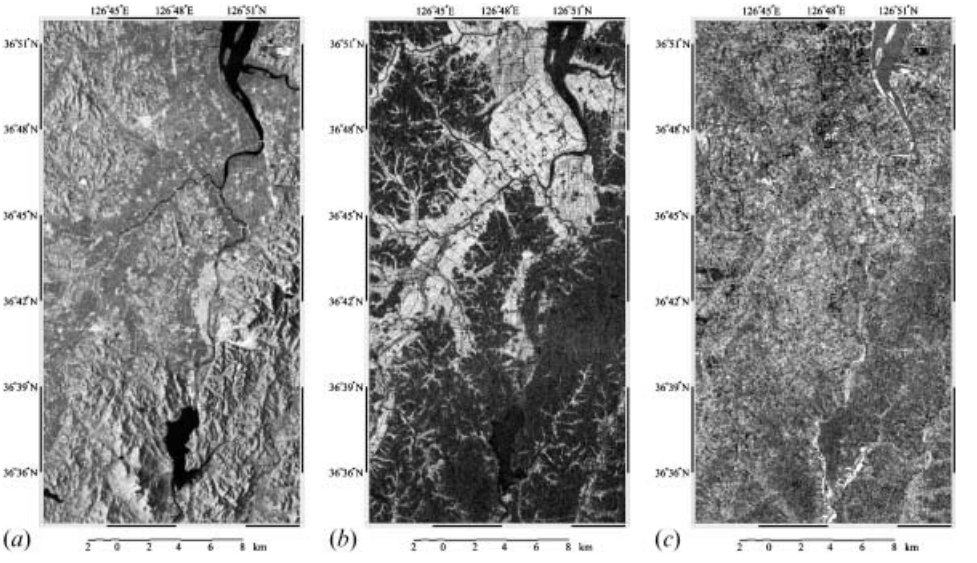


Figure 5. PCA-based features for Radarsat-1 data: (*a*) first PC, (*b*) second PC, and (*c*) third PC.

paddy fields. These results imply that the second PC reflects temporal changes in backscattering coefficient values and thus is similar to temporal variability. The third PC shows a cyclic pattern of negative and positive values. The first three PCs for the ENVISAT ASAR data sets are shown in figure 8. Unlike the temporal variability shown in figure 6(*b*), the second PC shows high and low values for paddy fields and water, respectively. As a result, their mutual discrimination is easily made from the second PC, although their temporal variability is similar. In the third PC, high values can be observed in water regions and relative lower values in paddy fields.

### 4.2 *Discrimination capability analysis*

Before classification, a histogram analysis of each input feature and the training data set was undertaken to qualitatively check the discrimination capability. Box plots based on the distribution of pixel values of features at training data locations are given in figure 9.

The overall results correspond to the discussion in §3. With SAR signal property-based features, water and built-up areas can be discerned from their average backscattering coefficient. The most distinguishing feature for the built-up class was seen to be long-term coherence, as expected. High temporal variability values from paddy fields in the Radarsat-1 data set mainly result from a backscattering change following variation in the physical conditions. In temporal variability derived from the ENVISAT ASAR data set, both water and paddy fields show a high value, but their ranges significantly overlap each other. As discussed before, the combined effects of VV polarization and the small incidence angle of the ENVISAT ASAR data set results in a differing intensity of temporal variability when compared with Radarsat-1 data results. In general, a high surface roughness and dense vegetation cover give a high VH/VV polarization ratio. Consequently, agricultural fields have an intermediate VH/VV ratio, whereas forest shows the highest VH/VV ratio of

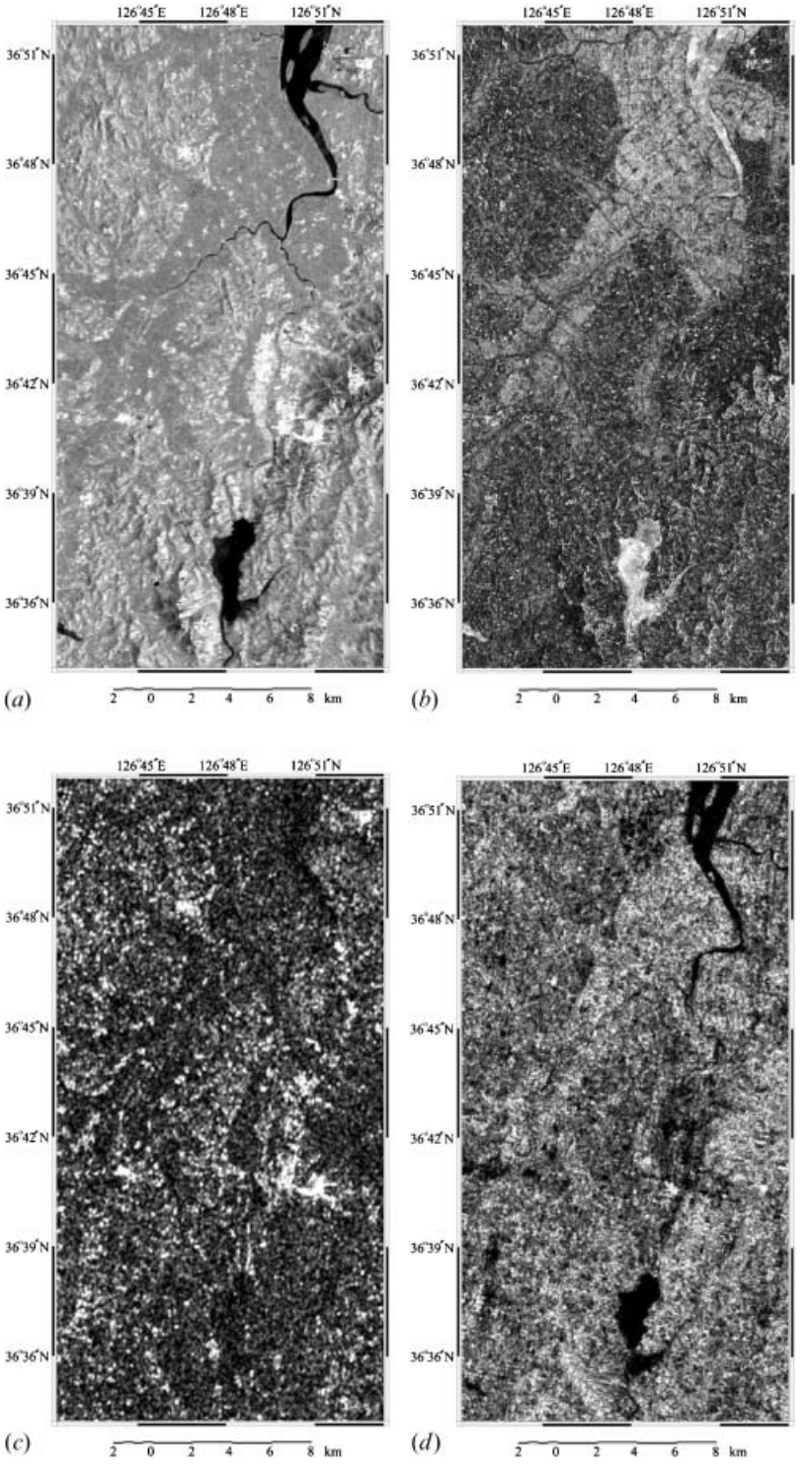


Figure 6. SAR signal property analysis-based features for ENVISAT ASAR data: (*a*) average backscattering coefficient, (*b*) temporal variability, (*c*) long-term coherence, and (*d*) VH/VV ratio.

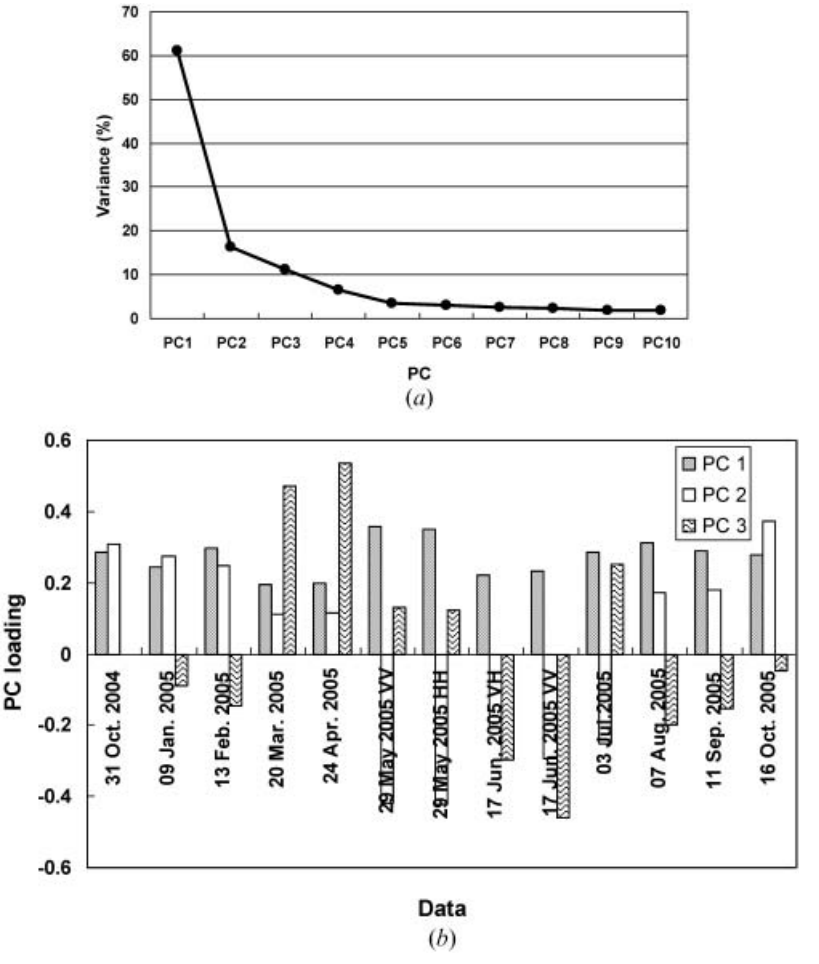


Figure 7. (*a*) Percentage of total variance explained by each PC of ENVISAT ASAR data and (*b*) principal-component loadings of input ENVISAT ASAR data.

natural targets (Wegmüller *et al.* 2003). In our VH/VV ratio, the distribution of forest significantly overlaps that of paddy fields, but the difference between forest and dry fields is distinct. Although a physical state seen only in the June data is considered, the result implies that the VH/VV ratio can be a useful feature for discrimination of forest and dry fields.

In considering PCA-based features, both water and built-up areas can be easily discriminated from the first PC, since this carries their similar information in the form of their average backscattering coefficients. The unique characteristic of the second PC derived from the ENVISAT ASAR data set is that a difference between water and paddy fields can be seen, as distinct from the temporal variability indication of the same data set. High values for dry fields can be observed from the third PC of the Radarsat-1 data set, and this may thus play an important role in the distinction of dry fields from forests. The additional information from PCA implies that the discrimination capability of PCA-based features would be superior to that using traditional SAR signal property analysis. Overall, the unique feature for discrimination of water, paddy fields, and built-up areas can be found in both

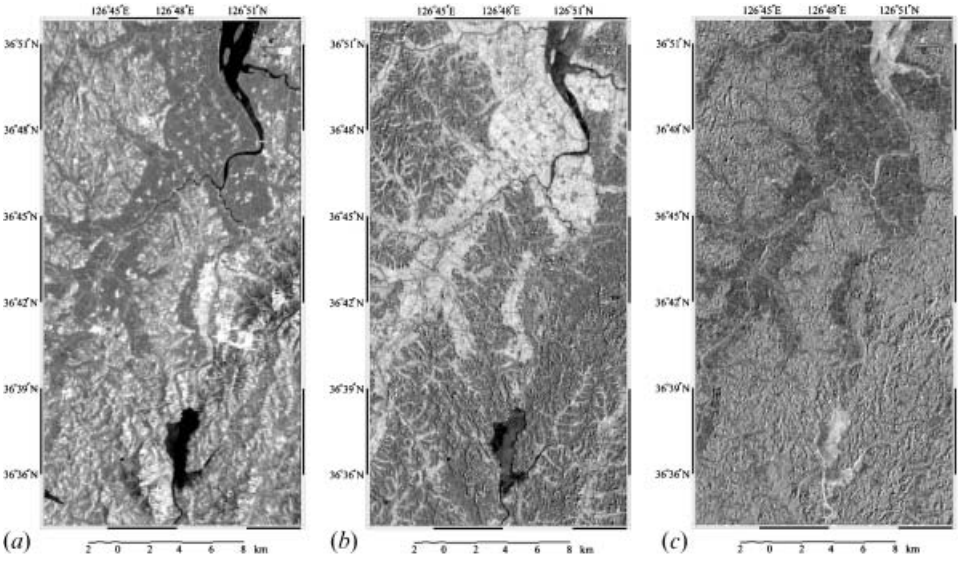


Figure 8. PCA-based features for ENVISAT ASAR data: (*a*) first PC, (*b*) second PC, and (*c*) third PC.

feature-extraction methodologies, but the best one for forest and dry fields is not clear. However, the VH/VV ratio and the third PC of the Radarsat-1 data set are good candidates for enabling discrimination to be made between forest and dry fields.

### 4.3 *Classification results*

The nine combination cases for the extracted features were considered in order to investigate the effects of a variety of feature combinations on land-cover classification capabilities, as shown in table 2. From those different combinations, it is possible to examine the difference between varying feature extraction procedures and the effect of combination with differing polarization. From cases numbered 1–6, the classification procedure corresponded to that using single multitemporal SAR sensor data sets. The integration of Radarsat-1 and ENVISAT ASAR data sets was carried out in cases 7–9.

The results of the combination cases considering the features from one sensor data set (i.e. from cases 1–6) were obtained via the MLP approach. For each feature combination, the MLP with input nodes corresponding to the number of the feature selected, one hidden layer, and five output nodes corresponding to the number of land-cover classes considered was trained by the error backpropagation learning algorithm. The number of neurons in the hidden layer was experimentally selected as five and the learning rate as 0.3. The estimates from the MLP were standardized by their sum to one. The integration cases from 7–9 were carried out by applying the tau model for a combination of the preposteriori probabilities derived from each of the sensor data sets through MLP. The a priori probability for each class was considered equal.

For classification-accuracy assessment, a confusion matrix was prepared, and related accuracy statistics (overall accuracy, user's accuracy, average accuracy, and kappa coefficient) were calculated by comparing the classification result and the

validation data set. The overall accuracy is the percentage of correctly classified pixels in the validation data set, and the user's accuracy is a measure of the probability that a classified pixel actually represents that class on the validation data set. The average accuracy is that derived from the user's accuracies obtained for each class. The kappa coefficient was also computed as a measure of the difference between the actual agreement and the change agreement (Lillesand and Kiefer 1994). The computed confusion matrices for typical cases are shown in table 3. Since the same validation data and the same number of samples were used in all experiments, the statistical significance of differences in classification accuracy statistics from various feature combination cases was evaluated by the McNemar test (Foody 2004).

Table 4 summarizes the classification results in terms of accuracy statistics with respect to various combination cases. The $Z$ statistic values computed from the McNemar test without continuity correction for the comparison of overall accuracy are also listed in table 5. The difference in overall accuracy between two comparison cases is significant at the 5% and 0.01% significance levels if $|Z|>1.96$ and 3.29, respectively. From the test, all the differences in overall accuracy with respect to case 9 were statistically significant at the 0.1% significance level.

When considering cases 1 and 2 (i.e. the use of features extracted from Radarsat-1 data), the accuracy of case 2 is higher than that of case 1. This improved accuracy of about 5% of overall accuracy and 7% of the kappa coefficient mainly came from the effect of the third PC. Among those cases using only ENVISAT features (i.e. cases 3, 4, 5, and 6), case 3 showed the worst classification accuracy and case 6 the best. The use of VH/VV ratio information affected the improved discrimination capabilities between forest and dry fields. However, the accuracy statistics for cases 5 and 6 were less than those for case 2. When comparing case 3 with case 5 (i.e. the differences between SAR signal analysis-based features and PCA-based ones in the ENVISAT ASAR data set), the improvement of classification accuracy was substantial for the combination of PCA-based features (case 5). An increase of about 7% in the kappa coefficient was achieved in combination case 5. Case 6 in which PCA-based features are combined with VH/VV ratio information showed the best classification accuracy for the ENVISAT ASAR data set. When comparing case 2 with case 5, PCA-based features of the Radarsat-1 data set showed a higher overall accuracy than those of the ENVISAT ASAR data. However, the overall accuracy in PCA-based features with the VH/VV ratio information of the ENVISAT ASAR data set (i.e. case 6) did not show a statistically significant difference from that of case 2. Accounting for the VH/VV ratio helped to complement the information content of PCA-based features from VV polarization data and consequently led to a similar overall accuracy, when compared with case 2.

For the integration of multiple polarization features, case 9 showed the best classification accuracy. Increases of about 5% of overall accuracy and 7% of the kappa coefficient were obtained, compared with case 2, which showed the best classification accuracy in the combination of single polarization features. The land-cover map from combination case 9 by the tau model is illustrated in figure 10. The collective use of HH, VH, and VV polarization as well as the effects of different incidence angles contributed to the improvement of classification accuracy. The accuracy of case 7 was slightly lower than that from case 2. However, the difference in overall accuracy between cases 2 and 7 was statistically insignificant at the 5% significance level. In other words, the integration of SAR signal analysis-based

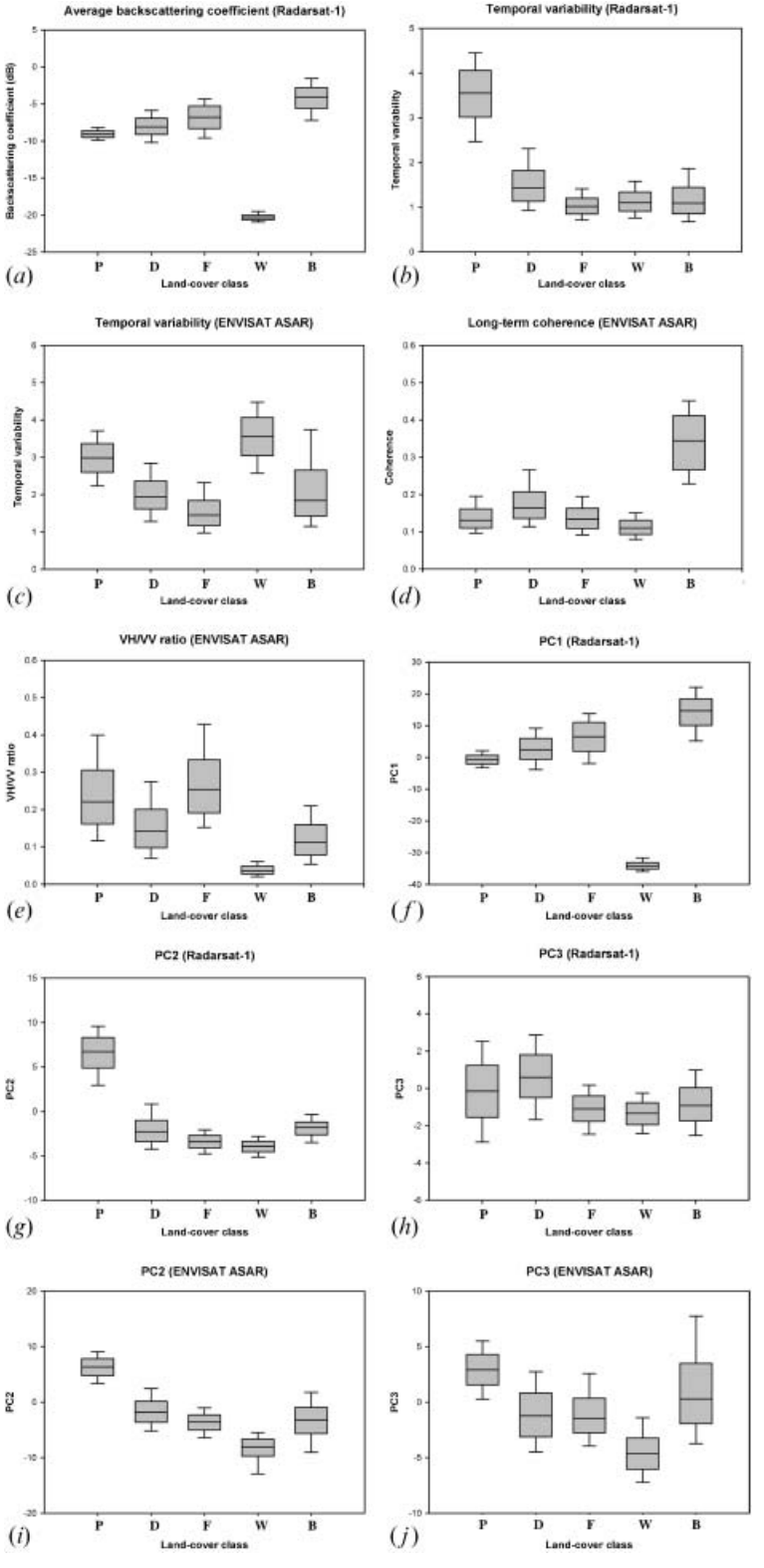

Table 2. Combination cases of various features.

| Case no. | Sensor | Combination |
|---|---|---|
| 1 | Radarsat-1 | Average backscattering coefficient, temporal variability, long-term coherence |
| 2 | | PC1, PC2, PC3 |
| 3 | ENVISAT ASAR | Average backscattering coefficient, temporal variability, long-term coherence |
| 4 | | Average backscattering coefficient, temporal variability, long-term coherence, VH backscattering coefficient, VH/VV ratio |
| 5 | | PC1, PC2, PC3 |
| 6 | | PC1, PC2, PC3, VH/VV ratio |
| 7 | Integration | Case 1, Case 3 |
| 8 | | Case 1, Case 4 |
| 9 | | Case 2, Case 6 |



Table 3. Confusion matrices for some combination cases.

| | | Reference data | | | | | |
|---|---|---|---|---|---|---|---|
| | | Paddy fields | Dry fields | Forest | Water | Built-up | Sum |
| *Case 2* | | | | | | | |
| Classification result | Paddy fields | 1223 | 51 | 0 | 10 | 0 | 1284 |
| | Dry fields | 32 | 388 | 313 | 18 | 7 | 1058 |
| | Forest | 0 | 87 | 824 | 1 | 0 | 912 |
| | Water | 0 | 0 | 0 | 299 | 0 | 299 |
| | Built-up | 0 | 67 | 9 | 0 | 371 | 447 |
| | Sum | 1255 | 893 | 1146 | 328 | 378 | 4000 |
| *Case 3* | | | | | | | |
| Classification result | Paddy fields | 1077 | 85 | 73 | 8 | 0 | 1243 |
| | Dry fields | 69 | 445 | 222 | 4 | 24 | 764 |
| | Forest | 108 | 280 | 848 | 8 | 0 | 1244 |
| | Water | 0 | 0 | 0 | 308 | 0 | 308 |
| | Built-up | 1 | 83 | 3 | 0 | 354 | 441 |
| | Sum | 1255 | 893 | 1146 | 328 | 378 | 4000 |
| *Case 9* | | | | | | | |
| Classification result | Paddy fields | 1254 | 42 | 1 | 4 | 0 | 1301 |
| | Dry fields | 1 | 642 | 93 | 12 | 3 | 751 |
| | Forest | 0 | 154 | 1051 | 4 | 5 | 1214 |
| | Water | 0 | 0 | 0 | 308 | 0 | 308 |
| | Built-up | 0 | 55 | 1 | 0 | 370 | 426 |
| | Sum | 1255 | 893 | 1146 | 328 | 378 | 4000 |

Figure 9. Box plots for the distribution of pixel values in each feature at training data locations. Five vertical lines are the 0. 1 quantile, lower quartile, median, upper quartile, and 0.9 quantile of the distributions of the values. Abbreviations of land-cover classes: P, paddy fields; D, dry fields; F, forest; W, water ; B, built-up areas. (*a*) average backscattering coefficient of Radarsat-1, (*b*) temporal variability of Radarsat-1, (*c*) temporal variability of ENVISAT ASAR, (*d*) long-term coherence of ENVISAT ASAR, (*e*) VH/VV ratio of ENVISAT ASAR, (*f*) first PC of Radarsat-1, (*g*) second PC of Radarsat-1, (*h*) third PC of Radarsat-1, (*i*) second PC of ENVISAT ASAR, and (*j*) third PC of ENVISAT ASAR.

Table 4. Accuracy statistics with respect to various feature combination cases.

| Case no. | Overall accuracy (%) | Average accuracy (%) | Kappa |
|---|---|---|---|
| 1 | 80.00 | 83.29 | 0.737 |
| 2 | 85.13 | 86.73 | 0.804 |
| 3 | 75.80 | 78.37 | 0.679 |
| 4 | 79.80 | 80.91 | 0.735 |
| 5 | 80.90 | 82.02 | 0.749 |
| 6 | 83.80 | 84.49 | 0.787 |
| 7 | 84.50 | 86.63 | 0.793 |
| 8 | 88.63 | 89.32 | 0.849 |
| 9 | 90.63 | 91.06 | 0.875 |



features from both data sets does not lead to an improvement of classification accuracy over case 2, which indicates the superiority of PCA-based features.

It is noteworthy that the classification accuracy between case 8 and case 9 is statistically significant, even at the 0.1% significance level, although the difference of classification accuracy was very small (i.e. 2% of overall accuracy and 0.026 of the kappa coefficient). The McNemar test is based on a binary $2 \times 2$ confusion matrix between correct and incorrect class allocation (Foody 2004). The large $Z$ value in the McNemar test means that the difference in non-diagonal elements (i.e. discordant pairs) is also large. As shown in figure 11, classwise accuracy values of all five land-cover classes in case 9 are greater than those in case 8. Many discordant pairs were generated from misclassification of forest and dry fields, and as a result, the statistically significant $Z$ value between cases 8 and 9 was obtained.

The effects of the integration of different polarization information can be accounted for by an examination of a classwise user's accuracy. Figure 11 shows the user's accuracy for each combination case of the tau model. The accuracy for water and paddy fields is very high in all cases. Compared with other classes, the lower classification accuracy of dry fields is mainly due to the cultivation in a restricted area of a complex variety of produce such as sweet potato, bean, ginger, sesame, and other crops, all with different phenological characteristics. Misclassification or confusion between dry fields and forest is very severe as shown in the confusion matrix (table 3). When considering cases 1 and 2 (i.e. the use of features extracted from Radarsat-1 data), an increase of about 10% in user accuracy for dry fields was achieved by considering case 2. For the ENVISAT ASAR data set, improved

Table 5. Summary of the McNemar test for the comparison of overall accuracy.

| Comparison case | 1 | 2 | 3 | 4 | 5 | 6 | 7 | 8 | 9 |
|---|---|---|---|---|---|---|---|---|---|
| 1 | – | 9.12 | 5.28 | **0.27** | **1.24** | 5.19 | 6.61 | 12.88 | 16.22 |
| 2 | | – | 11.77 | 7.15 | 5.79 | **1.90** | **0.90** | 5.48 | 10.37 |
| 3 | | | – | 6.32 | 8.03 | 11.89 | 12.49 | 18.26 | 20.60 |
| 4 | | | | – | 2.00 | 9.24 | 6.47 | 13.33 | 15.44 |
| 5 | | | | | – | 6.22 | 5.32 | 11.81 | 14.67 |
| 6 | | | | | | – | **1.03** | 7.94 | 11.01 |
| 7 | | | | | | | – | 9.33 | 11.06 |
| 8 | | | | | | | | – | 4.24 |
| 9 | | | | | | | | | – |

The figures in the table are absolute values of the $Z$ statistic. The comparison case in which the difference in overall accuracy is not statistically significant at the 5% significance level is shown in the bold cells.

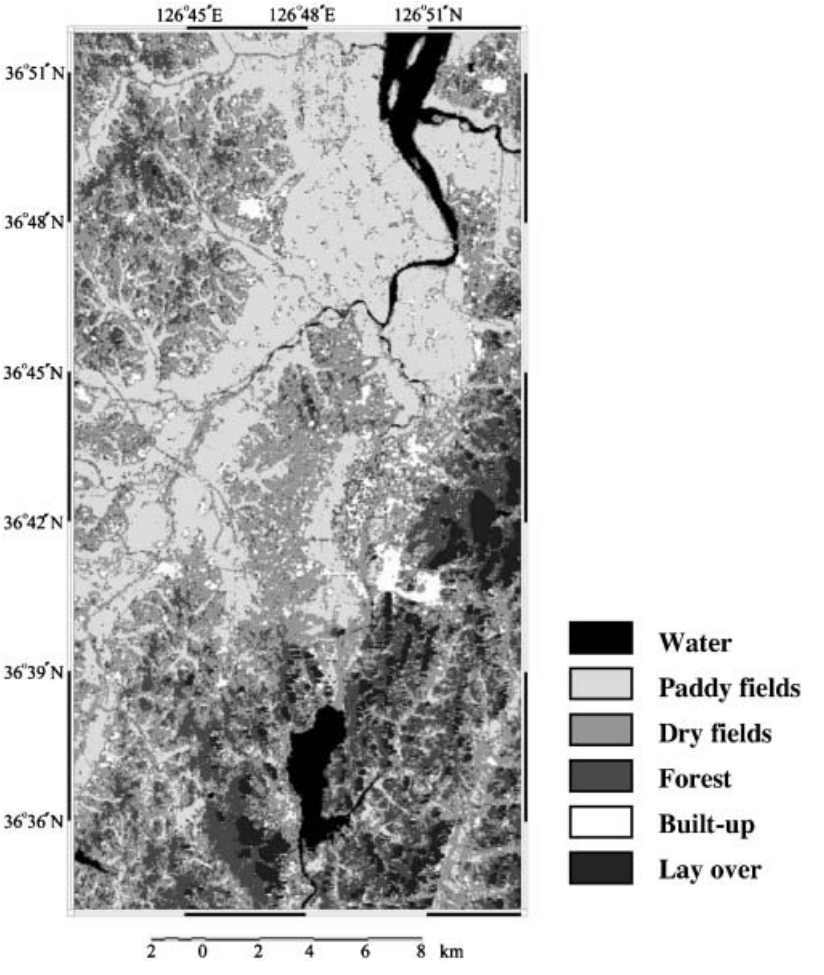


Figure 10. Land-cover map generated by using features of the case 9 and the tau model.

accuracy in dry fields can be obtained for case 6. The effects of the integration of different polarization information were the most significant in the dry fields. Although the overall accuracy of case 7 was similar to that from case 2 (table 4), the significant improvement of accuracy in dry fields was observed, which indicates that the integration of SAR signal analysis-based features from different sensor sets contributed to the improved accuracy in dry fields. The superiority of multiple polarization data (especially cross-polarization VH information) over features extracted from single polarization data alone is clearly demonstrated in the dry fields, although accuracy depends on the data used and the study area considered.

## 5. Conclusions

The use of multitemporal/polarization C-band SAR data and an advanced integration methodology with a feature extraction stage have been investigated. In addition to the joint use of multiple polarization data, the main novelty of the methodology presented herein lies in a comparison of the traditional feature extraction approach based on SAR signal property analysis with PCA.

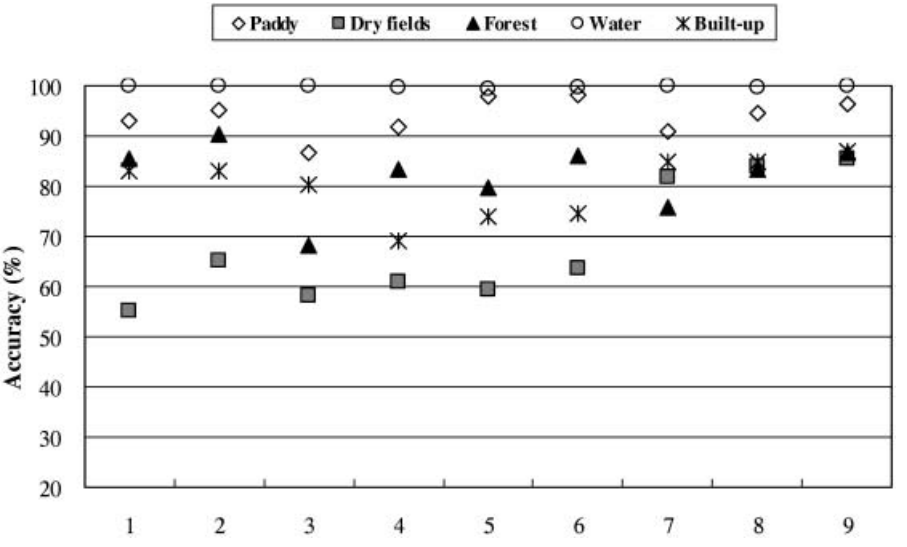


Figure 11. Classwise accuracy for each combination case.

From the case study for supervised land-cover classification using multitemporal Radarsat-1 and ENVISAT ASAR data, the combination of PCA-based features showed a higher classification accuracy than SAR signal property analysis. This study has demonstrated that PC loadings, which were not fully used in traditional PCA-based image analysis, could be used to interpret the contribution of each image to the PC, and thus PCA could be effectively applied to multiple remote sensing data analysis. The joint use of multiple polarization data resulted in improvement of the classification accuracy. Incidence angle and multiple polarization effects are also inherent in the integration of Radarsat-1 and ENVISAT ASAR data sets. In relation to the use of cross-polarization data, improvement of classification accuracy by incorporation of VH information into VV polarization data from ENVISAT ASAR data was observed. However, only one piece of VH information acquired in June was considered, and multitemporal behaviours of cross-polarization data were not fully investigated. Experiments with carefully designed multitemporal SAR data sets including multiple cross-polarization data should be undertaken to investigate thoroughly the effects on classification accuracy of different polarization data and alternative incidence angles.

From a methodological viewpoint, the tau model has a particular advantage in land-cover classification using multisensor data. In multisensor data fusion, it is very difficult to jointly model all the sensor data employing the same methodology. The optical data can be easily modelled with multivariate normal distributions, but SAR data should be modelled with other complex statistical distributions or with non-parametric approaches. If each batch of sensor data can be modelled with the best distribution or classification methodology within a probabilistic framework, the tau model can provide a combination framework in which the sensor-specific characteristics of different sensors can be accounted for.

The methodologies presented have been applied to the discrimination of five typical land-cover classes in a specific study area. Despite the superiority of the PCA-based feature extraction approach in this study, PCA is wholly based on the

statistical transformation of the data themselves and is thus heavily dependent on available data sets. More research is required to be devoted to extensive experiments that consider the discrimination of more complex land-cover classes in other regions to test the preliminary findings in this study. Multitemporal ground-based SAR investigations into various land-cover classes should be included in future work in order to interpret both the physical behaviour of the extracted features and dependency of results on alternative polarization states and incidence angles.

**Acknowledgements**

This work was supported in part by the internal research project of the Korea Institute of Geoscience and Mineral Resources, and in part by the Korea Research Council of Public Science and Technology. Three images among the ENVISAT ASAR data set used in this study were kindly provided by the Korea Aerospace Research Institute (KARI), Korea. We thank Professor Hoonyol Lee from the Kangwon National University, Korea for his valuable comments on coherence image generation and interpretation. Constructive comments and suggestions by two anonymous reviewers also helped us improve the presentation of this paper.



**References**

Angelis, C.F., Freitas, C.C., Valeriano, D.M. and Dutra, L.V., 2002, Multitemporal analysis of land use/land cover JERS-1 backscattering in the Brazilian tropical rainforest. *International Journal of Remote Sensing*, **23**, pp. 1231–1240.

Askne, J.I.H. and Hagberg, J., 1993, Potential of interferometric SAR for classification of land surfaces. In *Proceedings of the International Geoscience and Remote Sensing Symposium 1993*, pp. 985–987.

Bruzzone, L., Marconcini, M., Wegmüller, U. and Wiesmann, A., 2004, An advanced system for the automatic classification of multitemporal SAR images. *IEEE Transactions on Geoscience Remote Sensing*, **42**, pp. 1321–1334.

Caers, J., Avseth, P. and Mukerji, T., 2003, Geostatistical integration of rock physics, seismic amplitudes and geological models in North-Sea turbidite systems. *The Leading Edge*, **20**, pp. 308–312.

Carr, J.R. and De Miranda, F.P., 1998, The semivariogram in comparison to the co-occurrence matrix for classification of image texture. *IEEE Transactions on Geoscience Remote Sensing*, **36**, pp. 1945–1952.

Cloude, S.R. and Pottier, E., 1997, An entropy based classification scheme for land applications of polarimetric SAR. *IEEE Transactions on Geoscience Remote Sensing*, **35**, pp. 68–78.

De Grandi, G.F., Leysen, M., Lee, J.-S. and Schuler, D., 1997, Radar reflective estimation using multiple SAR scenes of the same target: techniques and applications. In *Proceedings of the International Geoscience and Remote Sensing Symposium 1997*, pp. 1047–1050.

Engdahl, M.E. and Hyypä, M., 2003, Land-cover classification using multitemporal ERS-1/2 InSAR data. *IEEE Transactions on Geoscience Remote Sensing*, **41**, pp. 1620–1628.

Ferro-Famil, L., Pottier, E. and Lee, J.-S., 2001, Unsupervised classification of multi-frequency and fully polarimetric SAR iamges based on the H/A/Alpha-Wishart classifier. *IEEE Transactions on Geoscience Remote Sensing*, **39**, pp. 2332–2342.

Foody, G.M., 2004, Thematic map comparison: evaluating the statistical significance of differences in classification accuracy. *Photogrammetric Engineering & Remote Sensing*, **70**, pp. 627–633.

Freeman, A. and Durden, S.L., 1998, A three-component scattering model for polarimetric SAR data. *IEEE Transactions on Geoscience Remote Sensing*, **36**, pp. 963–973.

JOURNEL, A.G., 2002, Combining knowledge from diverse sources: an alternative to traditional data independence hypotheses. *Mathematical Geology*, **34**, pp. 573–596.

KRISHNAN, S., 2004, Combining diverse and partially redundant information in the Earth sciences. PhD dissertation, Stanford University.

LEE, J.-S., GRUNES, M.R. and POTTIER, E., 2001, Quantitative comparison of classification capability: fully polarimetric versus dual and single-polarization SAR. *IEEE Transactions on Geoscience Remote Sensing*, **39**, pp. 2343–2351.

LILLESAND, T.M. and KIEFER, R.W., 1994, *Remote Sensing and Image Interpretation* (New York: Wiley).

PARK, N.-W., LEE, H. and CHI, K.-H., 2005, Feature extraction and fusion for land-cover discrimination with multitemporal SAR data. *Korean Journal of Remote Sensing*, **22**, pp. 145–162 (in Korean).

RICHARD, M. and LIPPMANN, R., 1991, Neural network classifiers estimate Bayesian a posteriory probabilities. *Neural Computation*, **3**, pp. 461–463.

STROZZI, T., DAMMERT, P.B.G., WEGMÜLLER, U., MARTINEZ, J.-M., ASKNE, J.I.H., BEAUDOIN, A. and HALLIKAINEN, M.T., 2000, Landuse mapping with ERS SAR interferometry. *IEEE Transactions on Geoscience Remote Sensing*, **38**, pp. 766–775.

TSO, B. and MATHER, P.M., 2001, *Classification Methods for Remotely Sensed Data* (London: Taylor & Francis).

ULABY, F.T. and DOBSON, M.C., 1988, *Handbook of Radar Scattering Statistics for Terrain* (Norwood, MA: Artech House).

WEGMÜLLER, U., STROZZI, T., WIESMANN, A. and WERNER, C., 2003, ENVISAT ASAR for land cover information. In *Proceedings of the International Geoscience and Remote Sensing Symposium 2003*, pp. 2996–2998.